

## Efficient energy transfer from Si clusters to Er<sup>3+</sup> in complex silicate glasses

Y. Lebour,<sup>a)</sup> P. Pellegrino, C. García, J. A. Moreno, and B. Garrido

EME, Department d'Electrónica, Universitat de Barcelona, Martí i Franquès 1, 08028 Barcelona, Spain

(Received 21 April 2006; accepted 12 July 2006; published online 6 October 2006)

We present an extensive study of the structural and optical emission properties in aluminum silicates and soda-lime silicates codoped with Si nanoclusters (Si-nc) and Er. Si excess of 5 and 15 at. % and Er concentrations ranging from  $2 \times 10^{19}$  up to  $6 \times 10^{20}$  cm<sup>-3</sup> were introduced by ion implantation. Thermal treatments at different temperatures were carried out before and after Er implantation. Structural characterization of the resulting structures was performed to obtain the layer composition and the size distribution of Si clusters. A comprehensive study has been carried out of the light emission as a function of the matrix characteristics, Si and Er contents, excitation wavelength, and power. Er emission at 1540 nm has been detected in all coimplanted glasses, with similar intensities. We estimated lifetimes ranging from 2.5 to 12 ms (depending on the Er dose and Si excess) and an effective excitation cross section of about  $1 \times 10^{-17}$  cm<sup>2</sup> at low fluxes that decreases at high pump power. By quantifying the amount of Er ions excited through Si-nc we find a fraction of 10% of the total Er concentration. Upconversion coefficients of about  $3 \times 10^{-18}$  cm<sup>-3</sup> s<sup>-1</sup> have been found for soda-lime glasses and one order of magnitude lower in aluminum silicates. © 2006 American Institute of Physics. [DOI: 10.1063/1.2356090]

### I. INTRODUCTION

The emission of Er<sup>3+</sup> around 1540 nm in silicate host matrices drives great interest as this wavelength corresponds to the minimum attenuation in silica-based optical fibers (third window). Er-doped fiber amplifiers have been widely deployed specially for long-haul optical communications in this spectral region. Nevertheless, concentration quenching effects and the small absorption cross section for Er excitation in silica ( $\sim 10^{-21}$  cm<sup>2</sup>) require the use of long devices. This limits the development of waveguide amplifiers of reduced size for local area networks and their integration with other photonic components. However, it has been found that the Er emission in silica is strongly enhanced by using Si nanoclusters (Si-nc) as sensitizers.<sup>1,2</sup> In such a codoped system, an increase of more than three orders of magnitude of the Er effective excitation cross section (up to  $10^{-17}$ – $10^{-16}$  cm<sup>2</sup>) for excitation in the visible has been reported.<sup>3,4</sup> Additionally, the broad absorption band of the Si clusters, used in this case to indirectly excite Er, enables the use of broadband light sources for excitation. In principle such results lead to expect that cheap flash lamp or light emitting diodes (LEDs) could efficiently replace the expensive 980 or 1480 nm lasers commonly used for pumping commercial Er-doped amplifiers. Furthermore, the Si clusters in the active region of the waveguide provide the index contrast necessary for the confinement of an optical mode at 1540 nm.<sup>5</sup> These properties offer the possibility to fabricate a compact, complementary metal-oxide semiconductor (CMOS) compatible, integrated and cost-effective erbium-doped waveguide amplifier (EDWA), where the active layer is composed by silica codoped with Si-nc and Er. Among the

recent progress in this field, it is worth to remark the achievement of optical gain by side excitation of the waveguide using LEDs by Han *et al.*<sup>6</sup> and the accomplishment of signal enhancement in Er-doped Si-nc waveguides reported by our group and coworkers.<sup>7</sup> On the other hand, the possibility to electrically excite such a system has been demonstrated,<sup>8</sup> opening the way to an electrically driven optical amplifier or laser.

Some reports exist in the literature about using complex silicate glasses as the host material for Er in the waveguides.<sup>9–12</sup> However, only two of them explore the Er emission properties once Si-nc are added to the original glass. Both of them account for enhanced Er emission from Si-rich Er doped alumino-silicate glasses, either using ion implantation to dope,<sup>11</sup> or cosputtering to elaborate the Si-rich glass.<sup>12</sup> No study is available yet about the influence of the Er concentration and the amount of Si excess on the emission properties of Er at 1540 nm in this or other complex silicate glasses.

In this work, we have explored the possibility to extend the mechanism of energy transfer from Si-nc to Er to two kinds of silicate glasses, namely, soda lime (SL) and aluminum silicates (AS). The interest in such composite glasses resides in their wide optical bandwidth at 1540 nm and the larger Er solubility when compared to that in pure silica. We have chosen two Si atomic excess (5% and 15%), and several Er concentrations in the range from  $2 \times 10^{19}$  to  $6 \times 10^{20}$  cm<sup>-3</sup>, and performed different thermal treatments in order to assess the best temperatures for promoting Si clustering and enhancing Er emission. A thorough structural characterization allowed us to investigate the formation of Si nanoclusters in the different silicate glasses and their impact on the emission properties of Er. A detailed analysis of the Er emission intensity either as a function of the photon excita-

<sup>a)</sup>Electronic mail: lebour@el.ub.es

tion flux or the time-resolved response allowed us to estimate excitation cross sections and lifetimes. By modeling the energy transfer from Si-nc to Er using the rate equations of the coupled system we have been able to estimate the upconversion coefficients in these glasses. Although being weaker than in pure silica, this process reduces the Er optical efficiency at high fluxes. Finally, we estimated that the fraction of excited Er ions at high fluxes is only about 10% of the total.

## II. EXPERIMENT

We used two kinds of glass wafers, provided by Corning: SL and AS. The ion implantation technique was used in order to incorporate Si excess and Er<sup>3+</sup> ions into the matrix. SRIM simulations have revealed that a multiimplantation scheme is necessary in order to get a uniform Si excess as a background to the subsequently implanted Er<sup>3+</sup> ions.

The wafers were processed in the following steps: (1) A Si ion multiple implantation at 35 and 70 keV was performed, with a resulting superficial layer (25–170 nm depth) with a uniform Si supersaturation in the silicate matrices. The doses were adjusted to get Si excess values of 5% and 15% atomic excess. (2) A first annealing step was performed in order to precipitate Si clusters and promote Si/SiO<sub>2</sub> phase separation. A temperature of 400 °C was applied for 15 min in a rapid-thermal process (RTP) furnace with controlled N<sub>2</sub> flow. (3) Er implantation was then performed at 200 keV, to adjust the Er peak right in the middle of the Si excess. The ion doses were varied from  $1 \times 10^{14}$  up to  $2.7 \times 10^{15}$  cm<sup>-2</sup> so that the resulting Er peak concentration (in the following indicated as [Er]) went from  $2 \times 10^{19}$  up to  $6 \times 10^{20}$  cm<sup>-3</sup>. (4) Afterwards, a second annealing step at different temperatures (hereafter referred to as postannealing) was intended to find the best tuning of annealing conditions in order to activate the Er atoms, and to maximize the photoluminescence emission at 1540 nm. While the duration and the N<sub>2</sub> flow were kept as in the first annealing step, the temperature was varied around the value used for the first thermal process. Three different runs were performed at relatively low temperatures of 350, 500, and 600 °C since the melting temperature for such glasses is about 700 °C.

Structural characterization of the resulting structures was carried out with dedicated experiments, such as secondary ion mass spectroscopy (SIMS), Raman spectroscopy, x-ray photoelectron spectroscopy (XPS), as well as transmission electron microscopy (TEM) in high resolution (HRTEM) and energy-filtered (EFTEM) configuration.

Systematic photoluminescence (PL) measurements (for excitations in and off resonant with an Er absorption band) were performed in order to draw a comprehensive study of the emission properties around the 1540 nm window. Room temperature PL measurements were performed in all the samples by using a He–Cd laser line at 325 nm with a power density of about 2 mW/cm<sup>2</sup> on the sample. The laser beam was modulated by a rotating chopper with frequencies around 11 Hz. The PL signal was detected in backscattering configuration with a liquid nitrogen-cooled Ge detector via a high resolution (0.02 nm) monochromator. The signal com-

ing from the detector was measured by a lock-in amplifier using the chopper frequency as a reference in order to improve the signal-to-noise ratio. All the spectra have been corrected for the spectral response of the system.

Time-resolved PL characterization was carried out in order to explore the dynamic response of the luminescence. The measurements were performed by using Ar laser with excitation at 488 nm (resonant line with an Er absorption band), or at 476 nm (out of resonance), in a large range of power. The 1540 nm Er emission was detected with an In-GaAs Hamamatsu photomultiplier and displayed on a digital Tektronix TDS 520B oscilloscope. From these measurements, we extracted the integrated PL emission, and the excitation rise and decay times by a single exponential fit. For an accurate study and quantification, great care was taken to calibrate the system and measure the incident power and the laser spot size on the sample.

## III. STRUCTURAL CHARACTERIZATION

A careful analysis of the material structure has been carried out in order to elucidate the modifications introduced and their effects on the optical performance of the resulting structures. The aggregation and nature of the introduced Si have been monitored by several techniques. As it has been reported for pure silica, the more suitable approach for maximizing the sensitization action of Si-nc is the formation of a high concentration of small amorphous Si clusters, randomly dispersed in the glass and in close proximity to the Er ions,<sup>13</sup> and at the same time avoiding the formation of Er-Si compounds.<sup>14</sup> In order to reach this ideal configuration a tight control of the Si-nc precipitation, cluster growth, and damage removal is required. For this purpose the thermal treatment has been divided in two steps, before and after the Er implantation. For the first annealing treatment, a short duration and a moderate temperature have been chosen. With this process we intended to suppress most of the implantation damage created during the high dose implantation, restoring the original matrix. At the same time we pursue the phase separation of the excess Si, but without reaching a full crystallization of the precipitates. Indeed the experimental evidences we obtained indicate that this goal can be reached by a proper choice of the thermal budget.

SIMS measurements performed on the as-implanted layers, after the Si<sup>+</sup> multi-implantation, reveal that the Si profile is quite uniform up to a depth of 200 nm, as expected by the SRIM simulations. Moreover, we detected a large structural modification in both glasses AS and SL, in respect to the unimplanted samples, due to the multiple collision cascades occurring during the implantation. The general trend observed is a depletion from the implanted region of all the light metallic elements (Li, Na, Al, etc.) which are basic components of these glasses. Such phenomena are attributed to the enhanced diffusivity of these metallic elements once ionized during the collision events.<sup>15</sup> It is also worth noticing that the postimplant thermal treatment restores an almost constant concentration of the metallic components all along the AS glass wafer, as depicted in Fig. 1 which represents SIMS profiles of the Al and Na distributions inside the im-

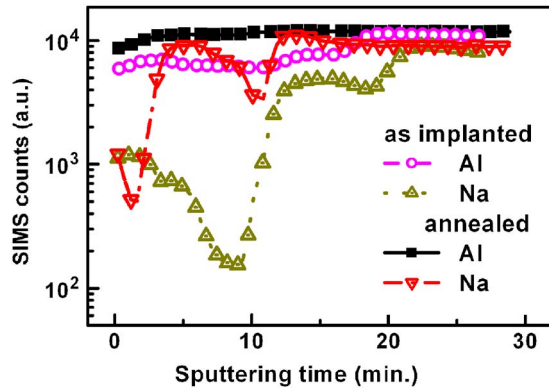


FIG. 1. (Color online) Al and Na distributions vs depth profile from SIMS, both in as-implanted and annealed AS layers.

planted layer. However, in the case of SL wafer the recorded profiles showed that the layers did not fully recover the original composition even after the annealing at the highest temperature (600 °C). Nonetheless, we did not detect any displacement of the Si implanted profile as a consequence of the annealing step neither in AS or SL glasses, implying that a rearrangement of the introduced Si atoms is discarded.

XPS analysis showed that a relevant part of the Si excess is already clustered after the annealing despite the relatively low temperature chosen (400 °C). A typical spectrum of Si 2*p* core level electrons photogenerated recorded in the implanted region is shown in Fig. 2 for the two kinds of matrices, together with its deconvolution into three different components corresponding to oxidation states Si<sup>+0</sup> (metallic Si), Si<sup>+1,2,3</sup> (suboxide band), and Si<sup>+4</sup> (stoichiometric Si oxide band). This provides a measure of the relative weight of each aggregation state for Si atoms in the layer, corresponding to

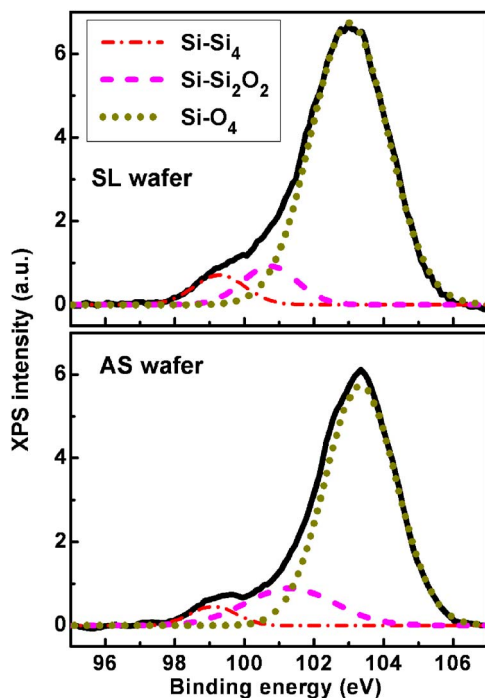


FIG. 2. (Color online) XPS spectrum of the Si 2*p* binding energies in SL (a) and AS (b) layers implanted with 15 at. % Si excess and annealed at 400 °C. Each spectrum has been fitted by Gaussian bands of three oxidation states.

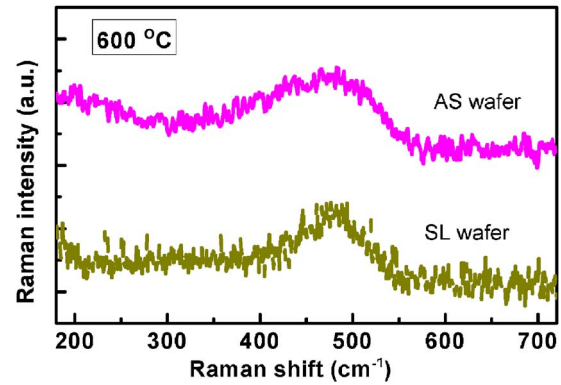


FIG. 3. (Color online) Raman spectra of the implanted layers after annealing at 600 °C.

Si clusters, SiO<sub>x</sub> and SiO<sub>2</sub>, respectively. From this evaluation we estimate that a fraction of more than one-third of all the implanted Si ions is already well aggregated into Si clusters in the case of AS wafers, while a slightly lower value has been found in SL.

Additional information on the Si precipitation in the wafers under study was obtained by the results of Raman scattering analysis. Figure 3 presents the Raman spectra from AS and SL wafers with 15 at. % Si excess and annealed at 600 °C. Regardless to the kind of matrix, the Raman spectrum shows the typical signature of amorphous silicon, with a characteristic resonance broadband peaked at 480 cm<sup>-1</sup>. The measured spectra imply that a phase separation occurs after the annealing step. However, it is not possible to quantify it as a partial or a complete one. Moreover, we deduce that the clustered Si is amorphous as the signature of crystalline Si at about 521 cm<sup>-1</sup> remains completely absent from the spectra of all the samples treated at these temperatures. These results are in good agreement with the XPS and SIMS analyses and show as a conclusion that a significant part of the excess Si is clustered after the first annealing step.

After the Er implantation and the final thermal treatment (postannealing) have been performed, the overall structural modifications have been investigated by EFTEM analysis. The Si-nc contrast on the TEM image was enhanced by filtering energetically the electron energy-loss spectra (EELS) by using a Gatan image filter (GIF 2000) around the Si plasmon, placed at 17 eV, which is well separated from the SiO<sub>2</sub> plasmon, placed at 22 eV. In the AS layers with the highest Si content (15 at. %) and postannealed at 350 °C a uniform Si cluster density has been detected, with average sizes of 2.5 nm (see Fig. 4). However, in all the samples implanted to the lowest Si dose (5 at. %), regardless of the host matrix, and in all SL glasses independently of the Si excess, no Si clusters have been detected, implying that their dimension is below the resolution of the technique, about 1 nm. Nevertheless, the existence of amorphous Si clusters in all these samples is supported by the Raman signal at 480 cm<sup>-1</sup> and the efficient absorption of visible radiation and energy transfer to the Er ions.

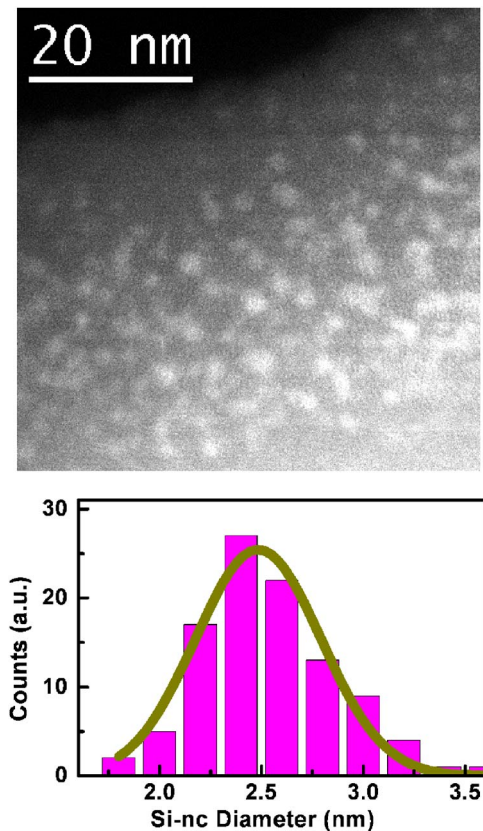


FIG. 4. (Color online) EFTEM image and the resulting Si-nc size distribution of a Si implanted AS layer after annealing at 500 °C.

#### IV. LUMINESCENCE CHARACTERIZATION

##### A. Er emission for nonresonant excitation

Room temperature PL measurements were carried out on all the samples using the HeCd laser line at 325 nm, being this wavelength out of resonance with absorption bands of Er. No emission at 1540 nm was detected from the glasses without Si excess. Such result shows clearly that the Er excitation is made via the Si clusters. This feature is well depicted in Fig. 5 which shows the emission spectra of AS and SL glasses with the same Er content (Er concentration of  $6 \times 10^{20} \text{ cm}^{-3}$ ) and a variable amount of Si excess. The differences of the spectra shape and their maxima are due to modifications of the Er local environment inside each kind of glass. The AS glasses show an emission spectrum of Er with a larger width and this means that optical amplifiers with a larger bandwidth can be fabricated from this material. The use of a nonresonant excitation line ensures that the only path for exciting the Er ions is through an energy transfer from exciton generated inside the Si clusters. Moreover, Fig. 5 features a clear dependence of the PL intensity on the silicon content in the Er-rich layers. This trend can be drawn irrespective of the Er concentration for the whole range explored in this work, i.e., from  $[\text{Er}] = 2 \times 10^{19} \text{ cm}^{-3}$  up to  $[\text{Er}] = 6 \times 10^{20} \text{ cm}^{-3}$ . As it will be shown later, this occurrence mainly reflects a higher fraction of Er ions effectively linked to Si-related sensitizing centers as the Si content is raised in the layers.

Isochronal annealing experiments (previously referred to as postannealing) have been performed in order to explore

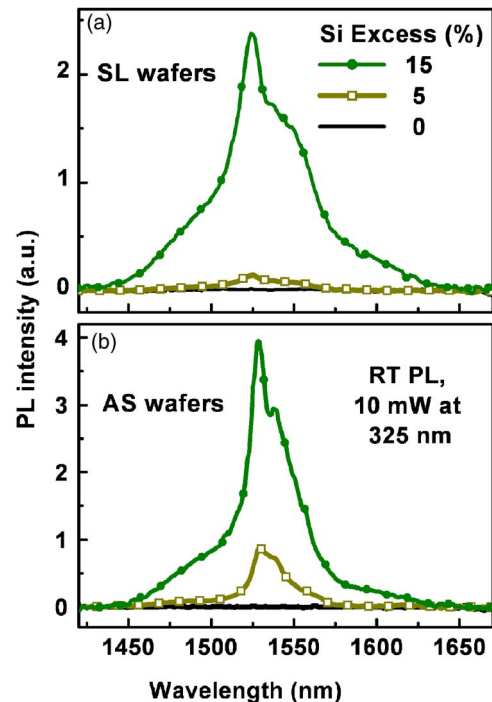


FIG. 5. (Color online) Room temperature photoluminescence spectra from coimplanted glass wafers excited out of resonance to an absorption band of Er: (a) from Al silicate wafers (b) from soda-lime wafers.

further the interaction between Er and Si-nc and maximize Er emission. A significant dependence on the processing temperature for the studied glasses has been observed only for high Er content ( $[\text{Er}] \geq 2 \times 10^{20} \text{ cm}^{-3}$ ) and in SL glasses, as depicted in Fig. 6. Moreover, while a moderate postannealing (500 °C) appears as the optimal value to maximize the PL enhancement in the case of AS for all Er concentrations, this value shifts to a higher temperature (600 °C) for the SL glasses. This can be attributed to the damage yields by the

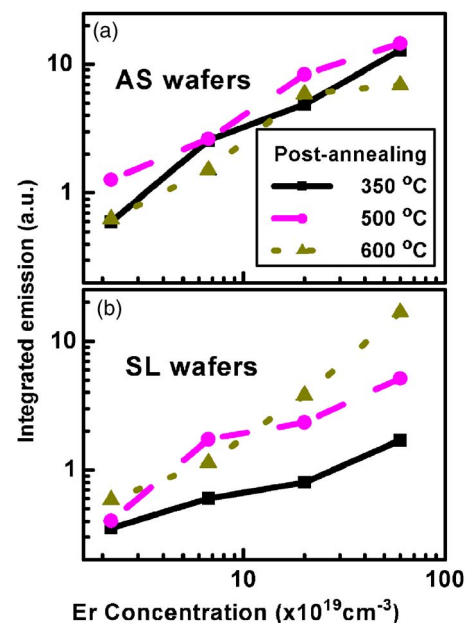


FIG. 6. (Color online) Evolution of the PL signal at 1540 nm with postimplantation annealing temperature for AS (a) and SL (b) layers coimplanted with 15 at. % Si excess and different Er doses.

implantation of Si and Er, and the recovery delays of the matrix after annealing in the case of SL wafers. It is worth to recall that SIMS showed a large structural modification in both glasses, which does recover after annealing in the case of AS wafers but not completely in SL glass. Besides, by EFTEM imaging we detected Si precipitates only in AS, though by Raman spectroscopy a precipitation of Si was detected in both kinds of glasses.

## B. Lifetimes and effective excitation cross section

In the previous section, the PL characterization showed that the energy absorbed by the Si clusters is transferred efficiently to a nearby Er ion for both kinds of complex glasses studied. The interaction between Si-nc and Er in silica has been explained as a dipole-dipole interaction between the Si-nc and Er atoms, with characteristic energy transfer times which are below  $1 \mu\text{s}$ .<sup>4</sup> These transfer times are much shorter than typical recombination times in Si-nc (several tens of microseconds) so the deexcitation of Si-nc occurs preferentially through energy transfer to Er. To determine characteristic parameters of the Si-nc and Er interaction we have explored the dynamic response of the processed layers to an optical excitation. Several time-resolved measurements were made in the 1540 nm window for different pump photon flux values in both kinds of samples. From the time evolution of the PL signal upon pulsed excitation we determined the lifetime ( $\tau_{\text{PL}}$ ) and the effective excitation cross section of Er ( $\sigma_{\text{abs}}$ ) in the following way: With good approximation we can consider the Er atomic system as a quasi-two-level system, as the decay times from the second and third excited levels (a few microseconds for silica) are much shorter than the decay times of the first excited level (millisecond). The rate equation for such a system with populations  $N_1$  and  $N_2$  for the fundamental and first excited levels, respectively, under a photon flux  $\varphi$  is

$$\frac{dN_2}{dt} = \sigma_{\text{abs}} N_1 \varphi - \frac{N_2}{\tau_{\text{PL}}} \quad (1)$$

So, under pulsed illumination, we obtain the lifetime from the transient decay of the PL and the plot of the rise time ( $\tau_{\text{rise}}$ ) versus photon flux gives the excitation cross section as

$$\frac{1}{\tau_{\text{rise}}} = \sigma_{\text{abs}} \varphi + \frac{1}{\tau_{\text{PL}}} \quad (2)$$

We found  $\tau_{\text{PL}}$  of around 12 ms for both glasses doped to the lowest Er concentration ( $[\text{Er}] = 2 \times 10^{19} \text{ cm}^{-3}$ ) and we observed that it progressively decreases as the Er content in the glass is raised, reaching 3 ms for the glasses doped to the highest Er concentration ( $[\text{Er}] = 6 \times 10^{20} \text{ cm}^{-3}$ ). The decrease of the excited state lifetime versus the Er dose mainly reflects the nonradiative recombination paths (defects and bond deformation) that the implantation and the Er itself introduce into the matrix, which does not fully recover after annealing. This is a cumulative effect; therefore, it is more important for the highest implanted dose ( $[\text{Er}] > 2 \times 10^{20} \text{ cm}^{-3}$ ).

The decay lifetimes for the SL glass coimplanted with 15 at. % Si excess and different Er concentrations are given in Fig. 7 as a function of the pump photon flux. The progres-

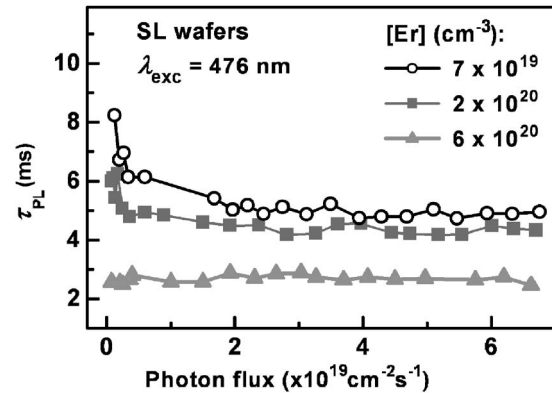


FIG. 7. Decay lifetimes ( $\tau_{\text{PL}}$ ) at 1540 nm vs the photon flux measured at nonresonant excitation (Ar laser line  $\lambda_{\text{exc}} = 476 \text{ nm}$ ), for different concentrations of Er codoped samples. The samples are SL wafers implanted with 15 at. % Si excess and annealed for 15 min at  $600^\circ \text{C}$  in  $\text{N}_2$ .

sive reduction of the lifetime with increasing flux is a clear signature of the fact that upconversion effects are important in these coimplanted glasses. We can model upconversion by adding to the rate equation (1) an additional term that accounts for Er–Er ion pair interactions in the excited state,

$$\frac{dN_2}{dt} = \sigma_{\text{abs}} N_1 \varphi - \frac{N_2}{\tau_{\text{PL}}} - C_{\text{up}} N_2^2, \quad (3)$$

where  $C_{\text{up}}$  is the so-called upconversion coefficient. From the dynamic response of the system such an upconversion process will be observed as a modified PL lifetime in the following way:

$$\frac{1}{\tau_{\text{PL}}(\varphi)} = \frac{1}{\tau_{\text{PL}}(0)} + C_{\text{up}} N_2(\varphi). \quad (4)$$

As the  $N_2(\varphi)$  dependence is that of a growing sigmoidal curve (stretched to high fluxes by  $C_{\text{up}}$ ), one expects a reduction of the lifetime with increasing flux, as the experimental results show. We will return later on to model further this effect and obtain the upconversion coefficients. Nevertheless, no dependence of PL lifetime with pumping power has been observed for the highest Er concentration, for which  $\tau_{\text{PL}}$  takes a value of about 2.8 ms. This flat dependence upon photon flux is also found for the other Er concentrations at relatively high photon fluxes, and the values obtained are 4.36 and 4.95 ms for Er concentrations of  $2 \times 10^{20}$  and  $7 \times 10^{19} \text{ cm}^{-3}$ , respectively. This saturation of the  $\tau_{\text{PL}}$  values for high fluxes together with Eq. (4) suggest that the number of excited Er ( $N_2$ ) tends to saturate at fluxes in the range of several  $10^{19}$  photons  $\text{cm}^{-2} \text{ s}^{-1}$ . The features shown in Fig. 7 have been also observed in the AS wafers.

As stated above, Eq. (2) provides a direct experimental estimation of the effective excitation cross section of Er from the linear fitting of the evolution of the rise time with the photon flux. A typical variation of the reciprocal rise time as a function of the photon flux is given in Fig. 8, which was obtained from a SL sample coimplanted with 15 at. % Si excess, ( $[\text{Er}] = 7 \times 10^{19} \text{ cm}^{-3}$ ), and postannealing at  $600^\circ \text{C}$ . We have estimated an effective excitation cross section of  $1.3 \times 10^{-17} \text{ cm}^2$ . For the two other Er concentrations ( $2 \times 10^{20}$  and  $6 \times 10^{20} \text{ cm}^{-3}$ ) we obtained excitation cross sec-

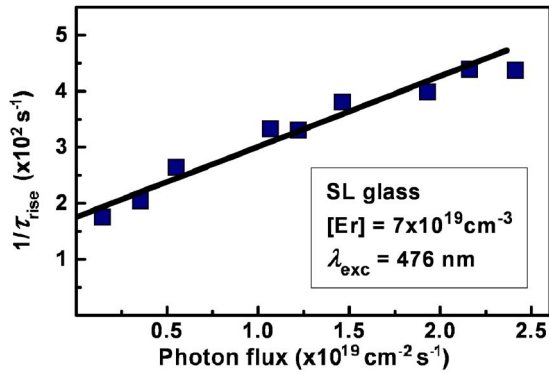


FIG. 8. (Color online) Variation of the reciprocal of the rise time with the photon flux at 476 nm from SL glass. A linear fit leads to an effective Er excitation cross section of about  $1.27 \times 10^{-17} \text{ cm}^2$ .

tions of  $3.5 \times 10^{-17}$  and  $5 \times 10^{-17} \text{ cm}^2$ , respectively. Similar values were obtained for the other host matrix (AS) and the same increasing trend with Er concentration, as reported in Table I. Moreover, a slightly increase of the effective excitation cross section with Er concentration and Si excess has been observed. This behavior can be understood considering that a higher Si content is directly related with a higher density and size of clusters and thus more Er ions are reached for efficient energy transfer.

### C. Power dependence of the Er emission

By looking at the variation of the PL peak as a function of the incident flux we observed that the 1540 nm emission has the same identical behavior for all the different [Er], apart from a rescaling factor proportional to the corresponding Er concentration. This feature is depicted in Fig. 9, which represents the evolution of the integrated intensity at 1540 nm versus the incident photon flux at 476 nm, in both AS and SL glasses, respectively. These samples were implanted with 15 at. % Si excess and annealed at 600 °C. One can see that the evolution of the PL intensity versus the pump

TABLE I. PL lifetimes and Er effective excitation cross section measured for different Er concentrations and Si excess. All the samples were postannealed at 600 °C except for those annealed at 500 °C. We used an off resonant excitation line (476 nm), except for that of 488 nm.

Er concentration ( $\times 10^{19} \text{ cm}^{-3}$ )	Si excess (at. %)	$\tau_{\text{PL}}$ (ms)	$\sigma$ ( $\times 10^{-17} \text{ cm}^2$ )
Soda lime			
7	15	4.95	1.27
20	15	4.56	3.5
60	15	2.8	5.05
60 <sup>a</sup>	15	2.28	5.77
60 <sup>b</sup>	15	2.96	1.72
60	5	9.36	...
Alumino silicates			
7	15	6.65	1.36
20	15	3.43	1.41
60	15	1.92	1.58
60	5	8.3	1.06

<sup>a</sup>The postannealing was 500 °C.

<sup>b</sup>The excitation line was 488 nm.

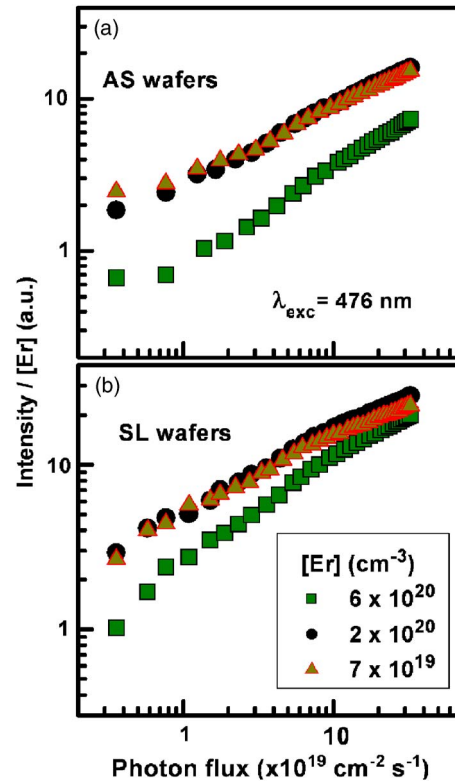


FIG. 9. (Color online) Variation of 1540 nm PL intensity as a function of the incident photon flux at 476 nm measured from (a) AS layer with 15 at. % Si excess, and (b) SL layer with 15 at. % Si excess for different Er concentrations.

flux is identical for different Er concentrations. Moreover, as far as this latter variable is equal or smaller than  $2 \times 10^{20} \text{ cm}^{-3}$ , the PL curves perfectly scale with [Er] (on Fig. 9 the PL intensity has been normalized to Er concentration, so that the curves overlap). Thus, for Er concentrations lower than this characteristic value, the emission per Er is the same (linear with [Er]), showing the good efficiency of the energy transfer in the system Si–Er clusters in these glasses. However, for the highest Er concentration ( $[\text{Er}] = 6 \times 10^{20} \text{ cm}^{-3}$ ), the relative PL intensity is lower, indicating that concentration quenching effects have already appeared. It is worth to note that once more this effect is more pronounced in SL glasses, due to their lower damage threshold.

### V. UPCONVERSION COEFFICIENTS AND ER EXCITED FRACTION

The value of the effective excitation cross section and the lifetimes we obtained demonstrate that population inversion in the Er–Si cluster waveguide amplifiers could be reached at very low pump power, much less than in the case of Er in silica based waveguides. In fact, without upconversion effects, the sigmoidal curve solution of Eq. (1) for steady state, with  $N_{\text{Er}}$  being the maximum amount of Er that can be excited through Si-nc, is

$$N_2(\varphi) = \frac{N_{\text{Er}}\varphi}{\varphi + 1/\sigma_{\text{abs}}\tau_{\text{PL}}}. \quad (5)$$

Thus,  $1/\sigma_{\text{abs}}\tau_{\text{PL}}$  is the characteristic flux for 50% inversion of the system and would be of the order of

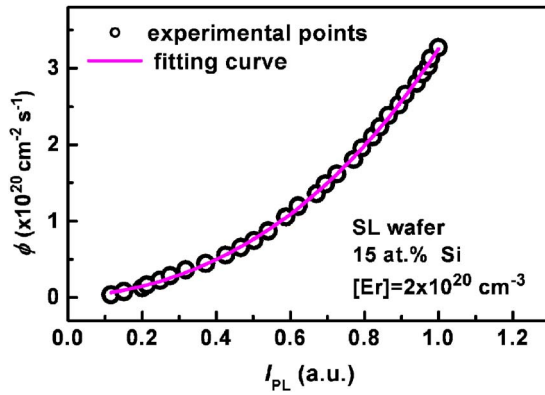


FIG. 10. (Color online) Pumping flux at 476 nm vs intensity of luminescence at 1540 nm for a codoped SL layer with 15 at. % Si and peak  $[Er] = 2 \times 10^{20} \text{ cm}^{-3}$ . The fitting curve has been calculated by using Eq. (7).

$10^{18} \text{ photons cm}^{-2} \text{ s}^{-1}$  if we inject the values obtained above. Nevertheless, for pure silica the values are similar, and gain measurements show that the fraction of inverted Er is much less for those photon fluxes. We can solve Eq. (3) in steady state conditions to get the population evolution with upconversion and we would get a stretched sigmoid; the net effect of upconversion is to increase the flux necessary for inversion,

$$N_2(\bar{\varphi}) = \frac{N_{Er}}{2C_{up}\tau_{PL}} [ -(\bar{\varphi} + 1) + \sqrt{(\bar{\varphi} + 1)^2 + 4N_{Er}C_{up}\tau_{PL}\bar{\varphi}} ] \quad \text{with } \bar{\varphi} = \sigma_{abs}\tau_{PL}\varphi. \quad (6)$$

As the PL intensity versus photon flux is given by  $I_{PL}(\varphi) = N_2(\varphi)/\tau_{rad}$  (where  $\tau_{rad}$  is the radiative lifetime), i.e., proportional to the excited state population, the fitting of  $I_{PL}$  in a sufficiently large range of photon fluxes can give us an estimation of  $C_{up}$ , together with the other parameters already measured such as excitation cross section and lifetime. We used Eq. (6) to arrange  $I_{PL}$  and the photon flux in the following way:

$$\varphi = \frac{AI_{PL} + BI_{PL}^2}{1 - CI_{PL}}, \quad (7)$$

where coefficients  $A$ ,  $B$ , and  $C$  are related to the modeling parameters in a simple way as follows:

$$\frac{C}{A} = \sigma_{abs}\tau_{PL} \quad \text{and} \quad \frac{B}{AC} = C_{up}\tau_{PL}N_{Er}. \quad (8)$$

A typical example of the good reproducibility of the experimental data by using the proposed model and Eq. (7) is provided in Fig. 10. As this kind of fittings require that  $I_{PL}$  bends to saturation (most of Er in the excited state) and as we can only obtain the product  $C_{up}N_{Er}$  from Eq. (8), first we have to assess the value of  $N_{Er}$ , as to say the Er density that can be excited through the Si-nc. Recently, Wojdak *et al.* found that in codoped silica samples with  $[Er] = 2 \times 10^{20} \text{ cm}^{-3}$  the excitable Er fraction was less than 3%.<sup>16</sup>

In order to provide an estimation of the Er population excitable via Si clusters, quantitative measurements of the photon flux emitted by the samples were performed. A com-

parison has been made of the PL of the samples to that of a 2 mm thick reference SL glass, with a uniform Er concentration equal to  $2 \times 10^{20} \text{ cm}^{-3}$  provided by Corning. The total emission of the latter had been independently evaluated with a calibrated optical spectrometer. Once the total emitted energy is known, the density of excited Er ions at any pump power can be easily calculated, knowing the layer thickness, and the radiative lifetime, whose value of 18 ms has been used. By this method, we estimate in our samples that the saturation value for the numbers of Er in the excited state is at most about 10% of the total amount of Er introduced into the wafers.

Finally, with that estimation for the Er coupled to the Si-nc, we obtain  $C_{up} \sim 4 \times 10^{-18} \text{ cm}^3 \text{ s}^{-1}$  for soda-lime glasses and  $\sim 3 \times 10^{-17} \text{ cm}^3 \text{ s}^{-1}$  for aluminosilicates. These values coincide with the ones found by Snoeks *et al.* in Er-doped SL glasses.<sup>17</sup> Larger  $C_{up}$  in AS glasses are expected with respect to SL glasses, as experimentally demonstrated in Er-doped bulk glasses.<sup>18</sup> This is due primarily to the higher optical cross sections of the relevant upconversion transitions found in AS matrix.<sup>19</sup> The value of  $C_{up}$  we determined is ten times higher than the one reported by Enrichi *et al.* for similar codoped AS structures.<sup>11</sup> It is possible that an erroneous hypothesis of considering as excitable the whole Er population brought them to an underestimation of  $C_{up}$  of an order of magnitude.

## VI. CONCLUSIONS

Complex silicate glasses doped with Si-nc and several Er doses have been characterized both from the structural and optical points of view. Si precipitates, with average sizes of 2.5 nm, have been detected by EFTEM analysis in AS doped with 15 at. % Si excess and annealed at low temperature (350 °C), while none was observed in the case of less doped wafers (5 at. %) and in all SL wafers, even after annealing at higher temperatures (600 °C). However, Raman spectroscopy provides a demonstration of precipitation of Si in both kinds of wafers. Intense emission, when comparing it to structures doped only with Er, has been detected in all coimplanted glasses. Thermal treatments have shown that a temperature around 500 °C seems to be the best to maximize the Er emission in the case of AS, while for SL wafers, it shifts to high temperature (600 °C), closer to the glass transition.

Time-resolved PL measurements yield lifetimes ranging from 2.5 to 12 ms (depending on the Er dose and Si excess) and an effective excitation cross section about  $1 \times 10^{-17} - 6 \times 10^{-17} \text{ cm}^2$ . This is several orders of magnitude higher than the Er direct absorption cross section (about  $10^{-21} \text{ cm}^2$ ). While this result provides a route to obtain gain in a waveguide, this can be done only if the amount of Er coupled to the Si-nc, which for our samples is of about 10% of the total introduced, can be increased up to the total of one. Thus, maximizing the concentration of the Er coupled to the Si-nc, as, for example, increasing the density of Si-nc, appears the ultimate challenge for the realization of an integrated optical waveguide amplifier based on Er-doped Si-rich glasses.

## ACKNOWLEDGMENTS

This work has been partly financed by the Spanish Project No. TIC2003-07464. The authors kindly acknowledge Dr. Jordi Arbiol from the University of Barcelona, Spain for EFTEM analysis and valuable discussions.

- <sup>1</sup>M. Fujii, M. Yoshida, Y. Kanzawa, S. Hayashi, and K. Yamamoto, *Appl. Phys. Lett.* **71**, 1198 (1997).  
<sup>2</sup>P. G. Kik and A. Polman, *J. Appl. Phys.* **88**, 1992 (2000).  
<sup>3</sup>A. J. Kenyon, C. E. Chryssou, C. W. Pitt, T. Shimizu-Iwayama, D. E. Hole, N. Sharma, and C. J. Humphreys, *J. Appl. Phys.* **91**, 367 (2002).  
<sup>4</sup>D. Pacifici, G. Franzó, F. Priolo, F. Iacona, and L. Dal Negro, *Phys. Rev. B* **67**, 245301 (2003).  
<sup>5</sup>J. A. Moreno *et al.*, *J. Appl. Phys.* **98**, 13523 (2005).  
<sup>6</sup>H.-S. Han, S.-Y. Seo, J. H. Shin, and N. Park, *Appl. Phys. Lett.* **81**, 3720 (2002).  
<sup>7</sup>N. Daldosso *et al.*, *Appl. Phys. Lett.* **86**, 261103 (2005).  
<sup>8</sup>F. Iacona *et al.*, *Appl. Phys. Lett.* **81**, 3242 (2002).  
<sup>9</sup>A. Polman, *J. Appl. Phys.* **82**, 1 (1997).  
<sup>10</sup>E. Snoeks, G. N. van den Hoven, and A. Polman, *J. Appl. Phys.* **73**, 8179 (1993).  
<sup>11</sup>F. Enrichi *et al.*, *J. Appl. Phys.* **96**, 3925 (2004).  
<sup>12</sup>F. Gourbilleau, P. Choppinet, C. Dufour, M. Levalois, R. Madelon, J. Vicens, R. Rizk, and M. Prassas, *Mater. Sci. Eng., B* **105**, 44 (2003).  
<sup>13</sup>G. Franzó, S. Boninelli, D. Pacifici, F. Priolo, F. Iacona, and C. Bongiorno, *Appl. Phys. Lett.* **82**, 3871 (2003).  
<sup>14</sup>J. C. Pivin, M. Jiménez de Castro, H. Hofmeister, and M. Sendova-Vassileva, *Mater. Sci. Eng., B* **97**, 13 (2003).  
<sup>15</sup>G. Battaglin, G. W. Arnold, G. Mattei, P. Mazzoldi, and J. C. Dran, *J. Appl. Phys.* **85**, 8040 (1999).  
<sup>16</sup>M. Wojdak *et al.*, *Phys. Rev. B* **69**, 233315 (2004).  
<sup>17</sup>E. Snoeks, G. N. van den Hoven, A. Polman, B. Hendriksen, M. B. J. Diemeer, and F. Priolo, *J. Opt. Soc. Am. B* **12**, 1470 (1995).  
<sup>18</sup>M. P. Hehlen, N. J. Cockroft, T. R. Gosnell, A. J. Bruce, G. Nykolak, and J. Shmulovich, *Opt. Lett.* **22**, 772 (1997).  
<sup>19</sup>J. E. Román, M. Hempstead, C. Ye, S. Nouh, P. Camy, P. Laborde, and C. Lermigniaux, *Appl. Phys. Lett.* **67**, 470 (1995).